Laminar flame structure of ethyl pentanoate at low and atmospheric-pressure: Experimental and kinetic modeling study

A.M. M Dmitriev, K.N. N Osipova, A.G. G Shmakov, T.A. A Bolshova, D.A. A Knyazkov, Pierre-Alexandre Glaude

Laminar flame structure of ethyl pentanoate at low and atmospheric-pressure: experimental and kinetic modeling study

A.M. Dmitriev[1,2,3], K.N. Osipova[1,2], A.G. Shmakov[1,2], T.A. Bolshova[1], D.A. Knyazkov[1,2,4], P.A. Glaude[3]

[1]Voevodsky Institute of Chemical Kinetics and Combustion, Novosibirsk 630090, Russia
[2]Novosibirsk State University, Novosibirsk 630090, Russia
[3]Université de Lorraine, École Nationale Supérieure des Industries Chimiques de Nancy, Laboratoire Réactions et Génie des Procédés, UMR CNRS 7274, Nancy Cedex 54001, France
[4]Institute of Applied Mathematics, Vladivostok 690041, Russia

Ethyl pentanoate (EPE) or ethyl valerate is considered a surrogate for biodiesel fuels and a potential fuel for spark ignition engines. Knowledge of its combustion chemistry is of great importance for the development of high-performance and environmentally friendly combustion devices fuelled with biofuels. In this work, a detailed chemical kinetic mechanism for the combustion of EPE is developed on the basis of a well-validated kinetic model proposed earlier for short ethyl esters up to ethyl propionate (by Sun et al.). The Sun et al. mechanism was augmented with primary oxidation reactions of ethyl butanoate and ethyl pentanoate and specific intermediates involved in these reactions. The proposed kinetic mechanism was validated against the new experimental data reported in this work on the chemical speciation of laminar premixed flames of stoichiometric EPE/O_2/Ar mixtures at low (50 Torr) and atmospheric pressures. The mechanism provided a good predictive capability for experimental mole fraction profiles of many flame intermediates. The new mechanism was also shown to predict well literature experimental data on laminar flame speeds of EPE/air mixtures in a range of equivalence ratios and pressures. The reported flame data can be used for validation of kinetic models for ethyl ester-based biofuels.

Keywords: ethyl pentanoate, ethyl valerate, biofuel, molecular beam mass spectrometry, premixed flame, chemical kinetic modeling, detailed chemical kinetic mechanism

1. Introduction

Global progress all over the world demands different sources of energy. Ester-based liquid biofuels seem to be very efficient in the context of fuel diversification. Like any alternative energy source, biofuels have special advantages and disadvantages, which are comprehensively discussed in various reviews with a focus on industrial [1], physicochemical [2], and economic [3] aspects. Transesterification with methanol yielding fatty acid *methyl* esters (FAMEs) was established as a dominant process for the treatment of oil based feedstock. Another less popular but promising strategy is transesterification with ethanol yielding fatty acid *ethyl* esters (FAEEs) [4]. This alcohol makes FAEE-fuel absolutely "green" since ethanol is non-toxic and derived from biomass [5]. Moreover, constantly developing technologies for bioethanol production make ethanol economically competitive with methanol [4]. From an academic point of view, the pyrolysis and combustion of FAEEs are also very interesting. Despite their apparent similarity to FAMEs, FAEEs have an additional path of destruction, the six-centered unimolecular elimination reaction yielding alkene and the corresponding carboxylic acid. The reaction has been actively discussed for ethyl propanoate [6] and ethyl butanoate [7] as examples. This unimolecular decomposition occurs at lower temperatures than H-abstraction by major flame radicals. Thus, FAEEs undergo faster decomposition than isomeric FAMEs, which was proved in a number of shock-tube [6,8,9] and jet-stirred reactor [7,10] experiments. However, the six-centered unimolecular decomposition reaction is not the only difference in combustion chemistry between FAME and FAEE. Although detailed chemical kinetic mechanisms of FAEE oxidation are of great scientific interest, there is still a lack of experimental data to validate and further improve these mechanisms.

Real ester-based biodiesels consist of heavy molecules with long C_{16}-C_{22} alkyl chains [2], which are very complex for detailed kinetic studies. To solve this problem, the hierarchical approach (from small to large) is usually applied. In the case of ethyl esters, only the lightest compounds are well studied. The shortest FAEE is ethyl formate, whose transformation kinetics not only on Earth but also in space is of great interest [11]. It has been extensively studied experimentally in a shock tube [9] and counterflow [12] and flat burners at different stoichiometric conditions [13,14]. Theoretical investigations of reactions of ethyl formate have also been performed by semi-empirical [15] methods and quantum chemistry methods [16]. Nonetheless, ethyl formate does not actually have alkyl chain and cannot be considered a model of a real biodiesel molecule. Thus, research interest has been shifted toward ethyl acetate and ethyl propanoate. These two FAEEs appear to be the most-studied small ethyl esters and are often investigated together in the same papers. Their ignition delay times [8] and pyrolysis [9] were studied in shock tubes; laminar flame speeds were measured in combustion chambers at atmospheric [17] and elevated [18] pressures and in counterflow burner [12] at atmospheric pressure. A lot of works on ethyl acetate and ethyl propanoate were dedicated to the chemical speciation in laminar flames: as a small additive to methane flame [19], as a single fuel in premixed flames at low [20] and atmospheric [21] pressures and in non-premixed conditions [22]. Together with experimental works several comprehensive studies using deep theoretical modeling have also been performed [6,14,15]. Nevertheless, the developed kinetic models are still being refined [23]. Although ethyl acetate and ethyl propanoate are far from the real biofuel molecules, all these experimental and theoretical studies have laid the groundwork for a detailed modeling of the oxidation of heavier ethyl esters. However, there are far fewer experimental studies of heavier FAEEs. Ethyl butanoate has been investigated experimentally and numerically in a shock tube [7], and in a tubular plug flow reactor [24]. The laminar flame velocity of ethyl butanoate was measured as well as that of ethyl acetate and ethyl propanoate [17], and its laminar flame structure

was measured and compared with that of methyl pentanoate [25]. Ethyl pentanoate is of particular practical interest and has therefore been the subject of many recent experimental studies [26–29]. Pentanoic esters will be discussed in more detail below. Heavier ethyl esters are quite complex subjects for detailed kinetic research because of their high boiling temperatures and viscosities and large masses. Unlike the light ethyl esters, heavy esters have not been studied systematically, and only a few studies kinetically examined molecules such as ethyl hexanoate [30], ethyl heptanoate, ethyl nonanoate [31] or ethyl levulinate [32].

On the one hand, fundamental kinetic studies of heavy esters provide a better understanding of the combustion chemistry of real biodiesel components; on the other hand, small esters are of interest as additives to gasoline fuel in spark ignition (SI) engines [25, 29]. Of particular interest are pentanoic (valeric) esters [33] since they can be produced from abundant lignocellulosic biomass [34,35]. Contino et al. [27] investigated the emissions and performance of a typical SI engine (PSA EP6 engine) fueled with pure methyl and ethyl pentanoates, 20% blends of these esters with reference fuel PRF95 and pure PRF95. In comparison with the reference fuel, no significant changes in emissions and performance were observed when using pentanoates. Moreover, these esters exhibit a higher research octane number [34], which thereby makes them a good fuel additive or alternative to gasoline.

As mentioned above, methyl esters have been studied much more extensively, and only a few kinetic studies of ethyl pentanoate (EPE) are available in the literature. Dayma et al. [26] first investigated EPE oxidation in a jet-stirred reactor (JSR) and laminar burning velocities of EPE/air mixtures at 1, 3, 5, and 10 bar in a combustion vessel. They proposed a detailed chemical kinetic mechanism based on the previously published kinetic model for the oxidation of C_1−C_5 hydrocarbons. In the following this work is cited as “Dayma et al.” for the sake of brevity. Since the experimental dataset on chemical speciation in flames provides a basis for validation and improvement of combustion kinetic models, two recent works [28,29] have focused on the chemical flame structure of EPE-fueled flames. Katshiatshia et al. [29] studied the laminar flame structures of three EPE/O_2/Ar mixtures at 55 mbar (41.3 Torr). Fuel-lean, near stoichiometric, and fuel-rich flames were examined by flame-sampling GC-analysis. Eight intermediate flame components, including formaldehyde, acetaldehyde, valeric, and formic acids, were detected. Surprisingly, acetylene was not detected in stoichiometric and fuel-lean conditions. Katshiatshia et al. [29] also proposed a mechanism based on their own UCL model [36] for the basic kinetics of C_0-C_4 species. The reaction kinetics of heavier compounds, including primary reactions of EPE decomposition, was taken from the mechanism of Dayma et al. Katshiatshia et al. [29] fitted, by trial and error, the rate constants of several reactions responsible for the decomposition of pentanoic acid (C_4H_9COOH) to match the experimental mole fraction of this species. The resulting model [29] well predicted mole fraction profiles for all major species; however, some discrepancies for intermediate species remained. Knyazkov et al. [28] also studied a low-pressure (20 Torr) premixed flat burner-stabilized flame of ethyl pentanoate by molecular-beam mass spectrometry with photoionization by vacuum ultraviolet radiation from the Advanced Light Source (ALS) in Berkeley, CA, USA. Mole fraction profiles of 43 flame components in stoichiometric EPE/O_2/Ar flame were measured. The authors reported significant discrepancies between the experimental data and the predictions of the Dayma et al. mechanism for many C_xH_y intermediates. However, it is worth noting that pentanoic acid was not identified in this work because the signal of the parent ion peak 102 corresponding to this compound was too low.

Thus, the first goal of this work was to verify the controversial results on the structure of low-pressure ethyl pentanoate flame by experimental examination of chemical speciation in a low-

pressure stoichiometric premixed EPE/O_2/Ar flame. The second goal was to extend the scarce experimental database for this fuel by investigation of a premixed EPE/O_2/Ar flame structure at atmospheric pressure. The third goal was to propose an updated detailed chemical kinetic mechanism for the combustion of ethyl pentanoate based on recent kinetic studies of ethyl esters. The mechanism was validated in this work against new data on the flame structure and the data on laminar burning velocities from [26]. A comparative analysis and a discussion of the mechanism are provided.

2. Experimental and modeling details

2.1. Experimental approach

Flame sampling is a challenging task because of the high temperature and species concentration gradients in the flame front. Studies of flame structures at atmospheric and elevated pressures are of high practical importance, however, low-pressure flame structure remains in demand. The main idea of studying low-pressure laminar flames is to stretch the flame zone to improve spatial resolution. In addition, low-pressure conditions significantly reduce the requirements for the pumping system. Both of these facts usually provide higher accuracy under low-pressure conditions. Low-pressure experiments help to better understand the main pathways of fuel decomposition, which usually remain the same at higher pressures. Thus, a combination of experiments at low and atmospheric pressures makes it possible to elucidate the most important reactions of fuel transformation under different conditions.

Pressure, Torr	Q_{EPE}, cm^3/s (NL/min)	Q_{O2}, cm^3/s (NL/min)	Q_{Ar}, cm^3/s (NL/min)	Q_{total}, cm^3/s (NL/min)	Q_{total}, g/cm^2s	Dilution*
50	2.37 (0.13)	22.57 (1.24)	75.17 (4.13)	100.1 (5.50)	0.00577	0.75
760	0.48 (0.026)	4.52 (0.248)	20 (1.099)	25 (1.373)	0.02033	0.8

*Dilution=Q_{Ar}/Q_{total},

Table 1. Flow rates of components of unburnt gas mixtures used in this study.

Two laminar premixed stoichiometric EPE/O_2/Ar flames stabilized at low and atmospheric pressures were studied in this work. The flow rates of unburnt gas mixture components are listed in Table 1. The low-pressure flame was investigated at the Laboratoire Réactions et Génie des Procédés (LRGP), Nancy, France. Online gas chromatography (GC) was used to obtain isomer-specific information for stable flame intermediates. The experimental setup and procedure were used in previous flame structure studies [37,38]; therefore, only key details are provided below. The flame was stabilized on a McKenna burner (60 mm diameter) at a pressure of 50 Torr. The burner was maintained at 333 K by thermostated water flow. Calibrated Bronkhorst High-Tech Mass Flow Controllers (MFC) were used to supply oxygen and argon. The flow of liquid EPE was controlled by a Bronkhorst mini CORI-FLOW MFC connected to a Bronkhorst Controlled Evaporator Mixer (CEM). Passing through the CEM heated up to 413 K, the liquid fuel was evaporated, mixed with oxygen and argon, and supplied through a heated line to the burner.

Flame sampling was carried out using a thin quartz probe with an orifice 100 μm in diameter and an inner angle of about 10°. The probe was attached to the evacuated heated line connected to the GC. Two gas chromatographs were used. Agilent 7890 A was equipped with HP-

Plot Q and HP-Molesieve columns to separate hydrocarbons, oxygenated compounds, and argon. Helium was used as a carrier gas. A flame ionization detector with a methanizer and a thermal conductivity detector were used. HP 5890 Series II with a Carbosphere column and a thermal conductivity detector was used to quantify H_2 and O_2. Argon was used as a carrier gas.

The GC-signal I_i of the *i*-th species was converted to the mole fraction X_i according to the formula $X_i = \frac{I_i}{S_i \times P_s}$, where S_i is the calibration coefficient of *i*-th component and P_s is the pressure of the sample injected to the chromatograph. To determine the coefficients S_i, we performed direct calibration measurements with gas mixtures of known composition. When direct calibration was not feasible, the corresponding coefficient S_i was estimated according to the number of carbon atoms in the molecule, considering that, thanks to the methanizer, the species corresponds to an alkane with the same number of carbon atoms. The uncertainties in the mole fraction measurements were about 5% for major compounds and 10% for minor products (<100 ppm).

The variation of temperature with height above the burner (HAB) was measured with a PtRh (6%)–PtRh (30%) thermocouple made of wires 100 μm in diameter. The thermocouple was covered with a BeO–Y_2O_3 ceramic coating [39] to avoid catalytic reactions on the thermocouple surface. An electrical compensation method [40] was employed to correct for radiative heat losses. The uncertainty of the temperature measurements was about ±80 K.

Atmospheric-pressure flame was studied using the MBMS setup at the Institute of Chemical Kinetics and Combustion (ICKC), Novosibirsk, Russia. A detailed description of the facility is provided in previous papers [41,42]. The flame was stabilized on a Botha-Spalding burner [43] (16 mm in diameter) at an atmospheric pressure p=760 Torr. The burner was maintained at a constant temperature of 368 K by water circulating through the cooling jacket of the burner. Flow rates of oxygen and argon were controlled by calibrated MFCs (MKS Instruments). Liquid EPE was supplied by a syringe pump to a vaporizer through a steel capillary. The vaporizer was a vessel made of Pyrex and filled with metal beads. It was maintained at a constant temperature of 410 K. This permitted complete gasification of liquid EPE in the vessel without ebullition in the capillary, which could cause instability of the fuel gas flow. An argon stream was passed through the vaporizer, drawing EPE vapor into the burner through the heated line.

The molecular-beam system provided direct sampling of gas from the flame. A molecular beam was formed by a quartz conical probe with an orifice at its tip. The orifice diameter was 80 μm, and the inner angle of the cone was 40°. The central part of the beam was cut by a skimmer and modulated by a chopper disk to distinguish between useful and background signals. The detection of flame components from a gas sample was carried out on an MS7302 quadrupole mass spectrometer with soft electron ionization (the deviation of electron energies was about ±0.25 eV). The electron ionization energy was adjusted individually for each component to achieve the best signal-to-noise ratio and minimize the contribution from fragmented ions of other species.

Mass peak intensity signals were converted to mole fractions of corresponding species using individual calibration factors. As in the low-pressure experiment, direct calibrations using pure gas mixtures were carried out to determine calibration factors for most stable species. For calibrated species (EPE, O_2, Ar, CH_4, C_2H_4, C_2H_6, C_3H_8, C_4H_6), mole fractions were determined with an uncertainty not exceeding ±15% (of the maximum mole fraction). For species that could not be calibrated directly, the calibration factors were estimated by the relative ionization cross-section (RICS)method [41,44] using the NIST Electron Impact Cross Section Database [45] to obtain values for the cross-sections for particular species. Due to the uncertainties associated with

the determination of the absolute ionization cross-sections, the mole fractions of species calibrated using the RICS method were determined with an error of about ±50%.

The flame temperature profile was measured with a Pt-PtRh (10%) thermocouple made of wires 50 µm in diameter. A thin SiO_2 coating was applied to the thermocouple surface to prevent catalytic effects. Correction for radiation heat losses was made according to the procedure proposed in [46,47]. The temperature was measured with an accuracy of ±50 K.

2.2. Modeling approach

Both flat flames were simulated numerically using the PREMIX code from the CHEMKIN II software [48] The measured temperature profiles were used to simulate the low-pressure and atmospheric-pressure flames.

Initially, the mechanism proposed by Dayma et al. was used for the calculations. This mechanism is the first detailed kinetic mechanism of EPE oxidation proposed in the literature. It is based on the mechanism for the oxidation of C_1−C_5 fuels [51][52][53] which was extended with EPE oxidation chemistry. Since only flames are studied in this work, low-temperature chemistry was removed from the mechanism. The full version of the mechanism includes 522 species and 2719 reactions, while the reduced version used in this work includes 232 species and 1845 reactions.

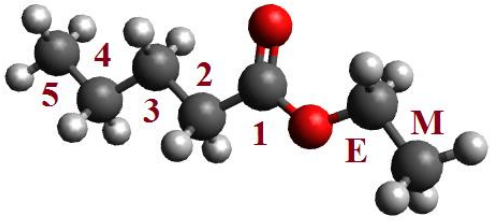

Figure 1. Ethyl pentanoate structure with C-atoms labeling.

The results of the calculations using the Dayma et al. mechanism showed unsatisfactory agreement with the experimental mole fraction profiles of the main C_2-C_3 intermediates. This could be associated with deficiencies in the basic hydrocarbon chemistry used in this mechanism. This motivated us to develop a new version of the EPE combustion mechanism free of this shortcoming. We started with the recent mechanism for the oxidation of small FAEEs proposed by Sun et al.[14] This mechanism was developed for the high-temperature oxidation of ethyl formate (EF), ethyl acetate (EA), and ethyl propionate (EP) using the AramcoMech 1.3 mechanism [52] for the base C_0-C_4 chemistry. The mechanism of Sun et al. was extended with the combustion chemistry of ethyl butanoate (EB) and EPE taken from the mechanism of Dayma et al. To construct a self-consistent mechanism, the rate constants of H-abstractions from the fuel by the main radicals (H, O, OH, and CH_3) in positions *E*, *M*, and *2* in EB and EPE (Figure 1 shows the structure of the EPE molecule with labeled carbon atoms) were taken the same as those used in the mechanism of Sun et al. It is worth noting that in the mechanism of Dayma et al., all three rate constants of H-atom abstractions in the 2^{nd}, 3^{rd}, and 4^{th} positions are similar. This is an acceptable approximation, but it is logical to assume that the rates of reactions in the 2^{nd} position should be influenced by the ester group. For the H-atom abstraction reactions in positions *E* and *M*, the rate constants seem to be similar to those proposed for ethyl esters with a shorter alkyl chain. To match the experimental results at low pressure (*see Section 3.1 Low-pressure flame*), the main reaction of ethanol formation $C_2H_5OH(+M)\leftrightarrows C_2H_5+OH(+M)$ was taken with the rate constant from the well-known

mechanism of Marinov [53]. All reactions whose rate constants were modified are listed in Table 2.

Reactions	*A (cm^3/mol·s)*	*n*	*E (cal/mol)*	*References*
EB+H=EB4J+H2	6.07E+10	1.18	8600.00	[54]
EB+H=EB3J+H2	1.43E+10	1.2	6050.00	[54]
EB+H=EB2J+H2	9.12E+09	1.22	4470.00	[54]
EB+H=EBMJ+H2	4.83E+10	1.22	9860.00	[54]
EB+H=EBEJ+H2	1.44E+10	1.25	5970.00	[54]
EB+OH=EB2J+H2O	4.87E+02	2.94	-2107.00	[55]
EB+OH=EBMJ+H2O	4.19E+01	3.72	-19.00	as EP in [14]
EB+OH=EBEJ+H2O	4.63E-02	4.32	-1640.00	as EP in [14]
EB+O=EB2J+OH	4.77E+04	2.71	2106.00	as MP in [56]
EB+O=EBMJ+OH	1.07E+03	3.6	6560.00	as EP in [14]
EB+O=EBEJ+OH	2.91E+02	3.6	3890.00	as EP in [14]
EB+CH3=EB2J+CH4	7.82E-05	4.92	3383.00	as MP in [56]
EB+CH3=EBMJ+CH4	1.77E-16	8.57	2637.00	as EP in [14]
EB+CH3=EBEJ+CH4	4.70E-25	11.28	-3624.00	as EP in [14]
EPE+H=EPE2J+H2	1.69E+10	1.21	4870.00	as EP in [54]
EPE+H=EPEMJ+H2	6.07E+11	0.93	10850.00	average from [54]
EPE+H=EPEEJ+H2	1.18E+10	1.27	5940.00	average from [54]
EPE+OH=EPE2J+H2O	9.15E+01	3.23	-1542.00	as MP in [56]
EPE+OH=EPEMJ+H2O	4.19E+01	3.72	-19.00	as EP in [14]
EPE+OH=EPEEJ+H2O	4.63E-02	4.32	-1640.00	as EP in [14]
EPE+O=EPE2J+OH	4.77E+04	2.71	2106.00	as MP in [56]
EPE+O=EPEMJ+OH	1.07E+03	3.6	6560.00	as EP in [14]
EPE+O=EPEEJ+OH	2.91E+02	3.6	3890.00	as EP in [14]
EPE+CH3=EPE2J+CH4	7.82E-05	4.92	3383.00	as MP in [56]
EPE+CH3=EPEMJ+CH4	1.77E-16	8.57	2637.00	as EP in [14]
EPE+CH3=EPEEJ+CH4	4.70E-25	11.28	-3624.00	as EP in [14]
C2H5OH(+M)=C2H5+OH(+M)	1.25E+23	-1.54	96005.00	[53]

Table 2. List of reactions with modified rate constants used in the proposed mechanism.

The resulting mechanism contains 320 species involved in 2027 reactions. The mechanism files in CHEMKIN format are attached as a Supplemental material. Both thermochemical and transport properties were taken from the mechanism of Sun et al. and expanded with data from the mechanism of Dayma. In the following, the measurement data are compared with the calculations using the mechanism proposed in this work and the mechanism of Dayma et al.

3. Results and discussion

3.1. Low-pressure flame

Low-pressure flat laminar flame of the EPE/O_2/Ar mixture was investigated at the LRGP. Mole fraction profiles of 24 individual species were measured using GC analysis. Among them are C_1-C_4 hydrocarbons, aldehydes, alcohols, ketones, carboxylic acids, and carbon oxides. The species detected and their molecular structures are listed in Table 2.

Formula	Species name	Structure	Formula	Species name	Structure
H_2	Hydrogen	H-H	C_3H_8	Propane	H_3C-CH_2-CH_3
O_2	Oxygen	O=O	n-C_4H_{10}	n-Butane	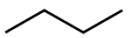
CO	Carbon monoxide	C≡O	iso-C_4H_{10}	Iso-Butane	
CO_2	Carbon dioxide	O=C=O	1-C_4H_8	1-Butene	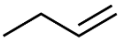
H_2O	Water		1,3-C_4H_6	1,3-Butadiene	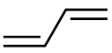
CH_4	Methane		CH_2O	Formaldehyde	
C_2H_2	Acetylene	HC≡CH	CH_3CHO	Acetaldehyde	
C_2H_4	Ethylene	H_2C=CH_2	C_2H_5OH	Ethanol	
C_2H_6	Ethane	H_3C-CH_3	CH_3COCH_3	Acetone	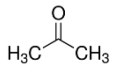
a-C_3H_4	Allene	H_2C=C=CH_2	$C_5H_8O_2$	Ethyl acrylate	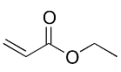
p-C_3H_4	Propyne	HC≡C-CH_3	C_4H_9COOH	Pentanoic acid	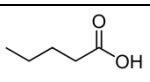

C_3H_6	Propene	$H_2C{=}CH{-}CH_3$	$C_7H_{14}O_2$	Ethyl pentanoate	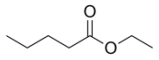

Table 3. List of species detected in the EPE/O_2/Ar flame at 50 Torr.

Experimental and simulated mole fraction profiles of reactants (EPE, O_2, Ar) and major flame products (H_2, H_2O, CO, CO_2) are presented in Fig. 2. The measured temperature profile is also plotted in this figure. Here and throughout all experimental profiles are represented by symbols, simulations with the mechanism of Dayma et al. are represented by solid lines, and simulations with the mechanism developed in this work by red dashed lines. The experimental mole fraction profiles of reactants and major products are reproduced well by both models. Only for the CO profile is a small discrepancy between the two models observed. The width of the flame zone at this pressure is about 4 mm. As can be seen from Fig. 2, some amount of oxygen is present in the post-flame zone even under stoichiometric conditions, according to the experimental data and simulations.

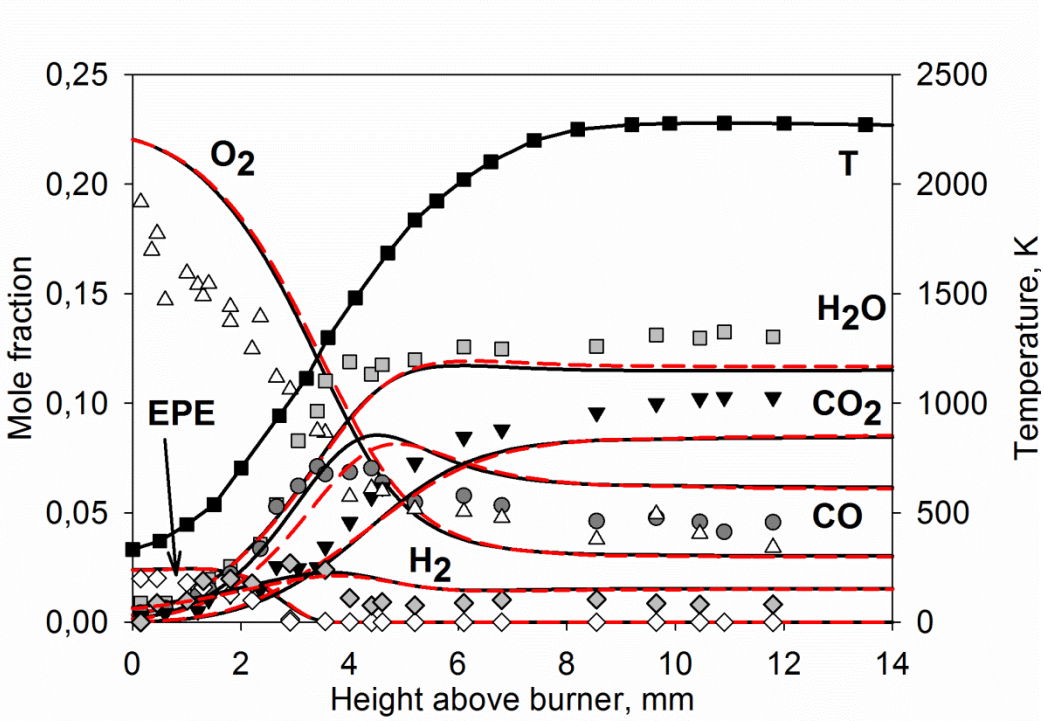

Figure 2. Measured temperature profile and mole fraction profiles of major components in the EPE/O_2/Ar flame at 50 Torr. Symbols: experimental data; solid lines: mechanism of Dayma et al.; red dashed lines: present mechanism. The temperature profile is shown by a black solid line with black squares.

Figure 3 shows the mole fraction profiles of C_1-C_4 hydrocarbons detected in the flame. The positions of the mole fraction peaks are generally well reproduced by both models; however, some noticeable differences between model predictions and experiments can be observed. Indeed, the present model describes very well the mole fraction profiles of acetylene, allene, and propyne, while the mechanism of Dayma et al. underpredicts the peak mole fractions of these species by a factor of 3-5. Conversely, the peak mole fractions of methane and ethane are slightly better predicted by the mechanism of Dayma et al., but the discrepancies between the predictions donot

exceed a factor of 1.5-2. The experimental mole fraction profiles of C_3H_6, C_3H_8, n-C_4H_{10}, and 1-C_4H_8 are accurately reproduced by both models.

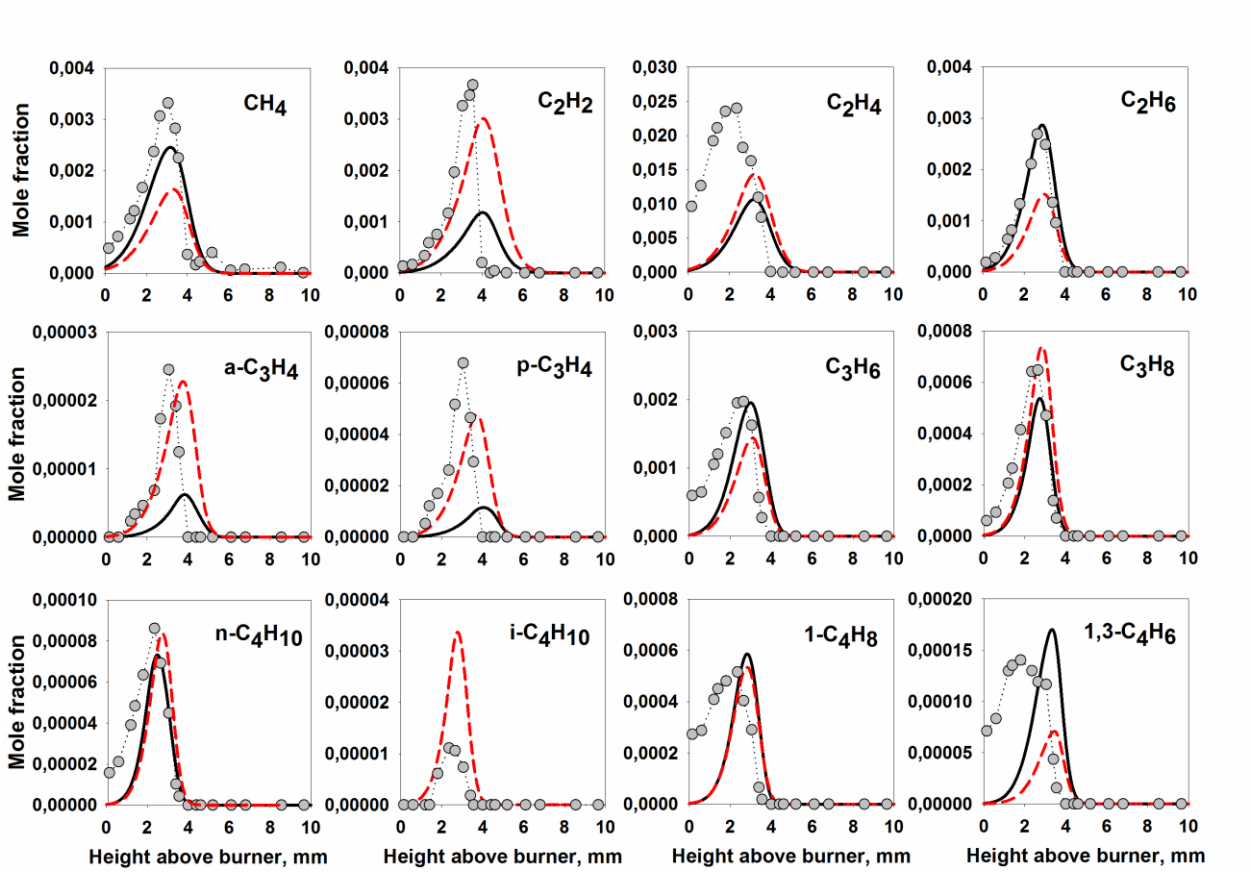

Figure 3. Mole fraction profiles of C_1-C_4 hydrocarbons in the EPE/O_2/Ar flame at 50 Torr. Symbols: experimental data; solid lines: mechanism of Dayma et al.; red dashed lines: present mechanism.

The experimental peak mole fractions of C_2H_4, i-C_4H_{10}, and 1.3-C_4H_6 are poorly reproduced by both kinetic models. The measured peak mole fraction of ethylene is significantly higher than the simulated one, and its position is shifted toward the burner. Iso-butane is formed in an amount 10 times smaller than that of n-butaneand is probablytherefore not included in the mechanism of Dayma. However, iso-butane is taken into account in the Aramco 1,3 mechanism and is thus included in the proposed mechanism; the mechanism reproduces well the iso-butane profile position, but overestimates its peak mole fraction by a factor of 3. Both simulations of 1,3-butadiene do not match the experimental data on the position and peak mole fraction: the experimental profile is shifted toward the burner surface and exhibit a noticeable concentration near the burner. The same shift and non-zero concentration near the burner are observed for the profile of 1-butene, since 1,3-C_4H_6 is formed from 1-C_4H_8. This problem has been discussed previously [28] for many measured peaks. It has been found that the mechanism of Dayma et al. leads to significant underestimations in the vicinity of the burner, which have been attributed to unclarity in the unimolecular decomposition of fuel radicals. Indeed, 1-C_4H_8 is formed predominantly from the EPE3J fuel radical, so that its kinetics should be revised.

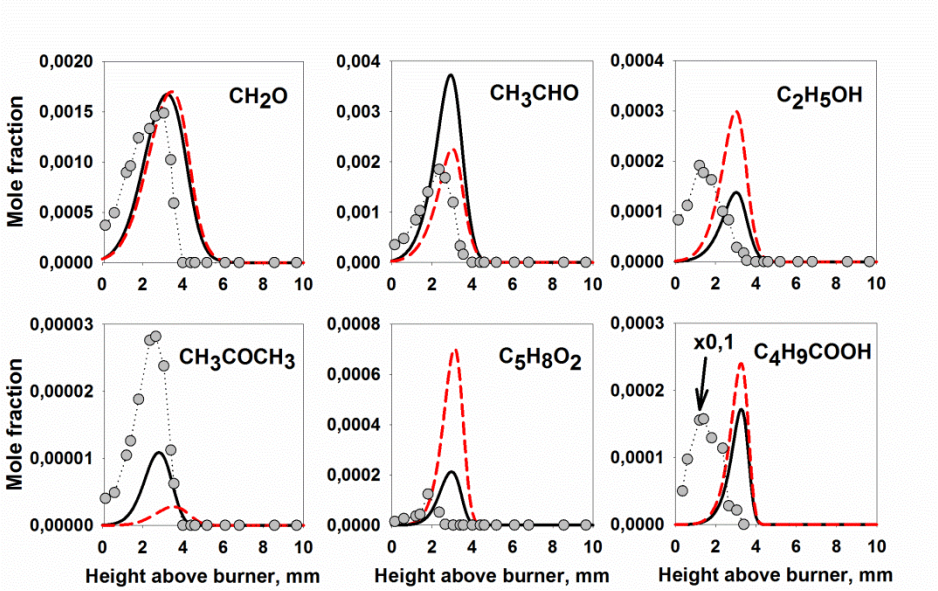

Figure 4. Mole fraction profiles of oxygenated intermediates in the EPE/O_2/Ar flame at 50 Torr. Symbols: experimental data; solid lines: mechanism of Dayma et al.; dashed lines: the present mechanism.

All detected oxygenated intermediates are shown in Fig. 4. As can be seen, the peak mole fraction of acetaldehyde is higher than that of formaldehyde. This is a typical result for FAEE flames due to the breakaway of the ethyl ester part of the primary fuel radical, while in FAME flames, the ester part is shorter (methyl) and more formaldehyde can be found. The developed model predicts the peak mole fraction of acetaldehyde much better than does the mechanism of Dayma, which overestimates it by a factor of almost two.. The experimental peak mole fraction of ethanol is in satisfactory agreement with the models, but its position is shifted toward the burner surface as in the case of 1-butene and 1,3-butadiene. It is worth noting that originally the basic sub-mechanism (AramcoMech 1.3) underpredicted the peak mole fraction of ethanol by a factor of almost 10.To improve the agreement for ethanol, we replaced the rate constant of the main reaction of ethanol formation ($C_2H_5OH(+M) \leftrightarrows C_2H_5+OH(+M)$) by the rate constant from the mechanism of Marinov [53]. It should be noted that the full sub-mechanism of Marinov for ethanol kinetics is included in the mechanism of Dayma et al.

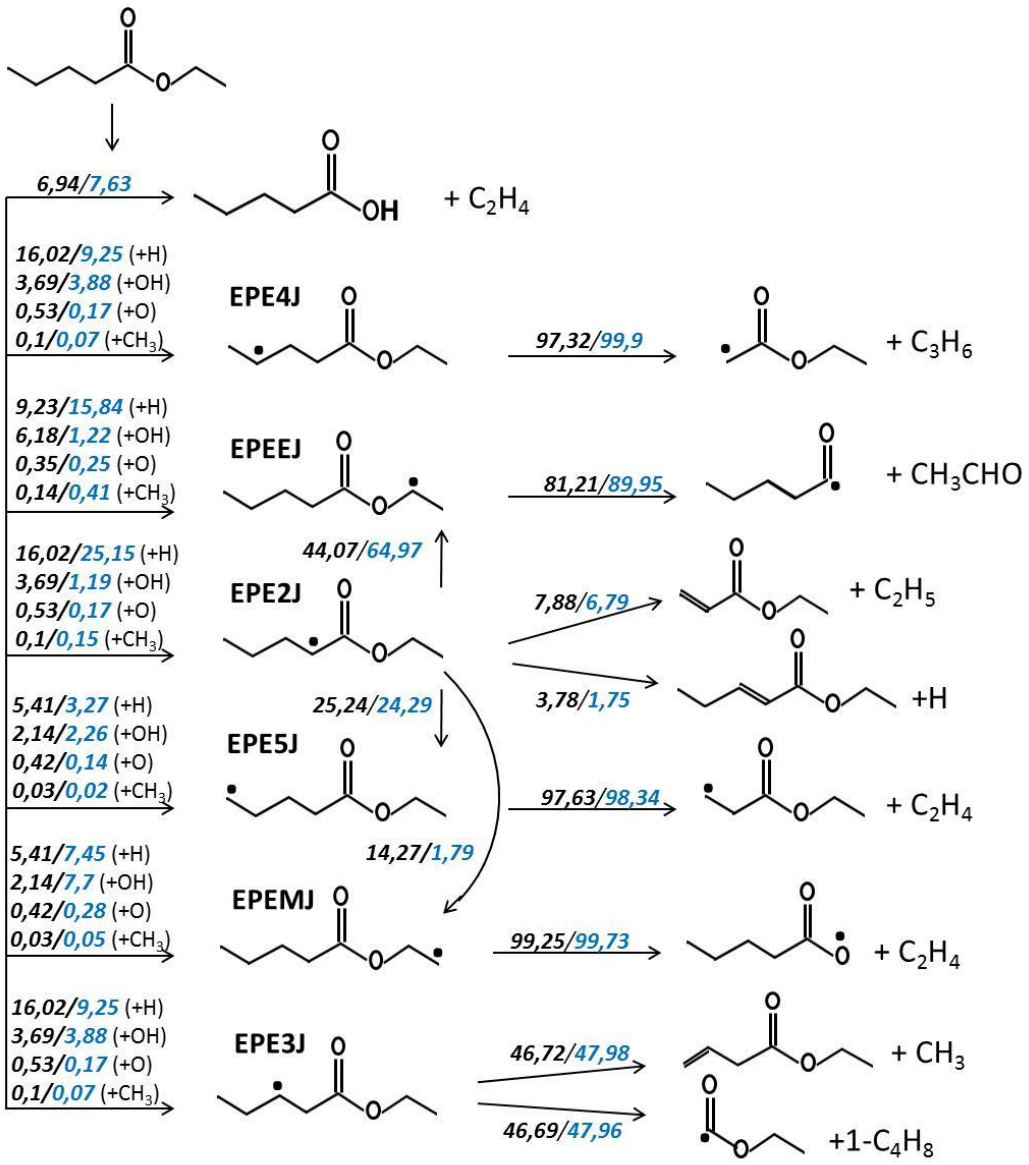

Figure 5. Integrated ROP analysis of the primary pathways of EPE destruction at 50 Torr. Black values: percentage contribution to the total consumption of a particularcomponent according to the model of Dayma et al.; blue values: according to the present model.

The mole fraction profiles of acetone, ethyl acrylate, and valeric acid are less accurately predicted by both models. The peak mole fraction of acetone is underpredicted by a factor of 3 by the Dayma et al. mechanism and by a factor of almost 5 by the present mechanism. The mole fraction profile of ethyl acrylate is fairly well predicted by the mechanism of Dayma et al., but it is overestimated by a factor of 3.5 by the present model. For valeric acid, as for ethylene, the experimental peak mole fraction is unreasonably high. In addition, its position is shifted toward the burner, similarly to the position of the ethylene peak mole fraction. Both of these compounds can be formed by the unimolecular decomposition of EPE via the six-centered unimolecular elimination reaction discussed in the Introduction. We assume that the observed discrepancy for valeric acid and ethylene can be explained by the possible transformation of the sample in the

probe. In particular, some decomposition of EPE may occur in the probe due to insufficient cooling of the sample (if the temperature drop in the probe is not fast enough). Note that the heated transfer line from the probe to the GC does not cause this transformation, since calibration measurements using a cold gas mixture of known composition (EPE/Ar) did not show any decomposition of the fuel.

To get insights into the primary pathways of fuel destruction, we performed an analysis of integrated rates of production (ROP) for both models (seeFig. 5. The analysis was carried out in a manner similar to that used in our previous works[57,58]. In the diagram in Fig. 5, the values on the lines represent the contributions (for different mechanisms) of the integrated rate of each pathway to the total integrated rate of consumption of a particular species in the entire flame. Black values correspond to the integrated ROP analysis with the model of Dayma, and blue values to the analysis using the mechanism proposed in the present study.

As seen from Fig. 5, in contrast to short ethyl esters such as EA and EP, the impact of unimolecular decomposition on the destruction of EPE is marginal compared to H-abstraction pathways under flame conditions. This is a consequence of the elongation of the alkyl chain in the homologous series of FAEEs; i.e., the longer the chain, the larger the number of possible positions for radical attacks. Thus, most of EPE in the stoichiometric flame is consumed via H-abstraction reactions with the main flame radicals (H, OH, O and CH_3). As can be seen from Fig. 5, the use of recent rate constants increased the impact of H-abstraction by the Ḣ-radical yielding EPEEJ and EPE2J fuel radicals. The relative impact of H-abstraction yielding EPE2J is higher than that yielding EPE3J and EPE4J. The same trens was observed for the rate constants of H-abstraction with Ḣ-radicals from EB molecules in the work of Wang et al. [54] According to the theoretical calculations, at a temperature less than 1300 K, the rate constant of H-abstraction from the α carbon (2^{nd} position) is higher than that from the β and γ carbons (3^{rd} and 4^{th} positions). According to the analysis performed, the isomerization of EPE2J to EPEEJ increased, which also ledto a redistribution of the primary decomposition pathways. In particular, the simulation of the acetaldehyde profile in the recent mechanism was in better agreement with the experimental data.

In a recent paper by Namysl et al. [59], a new kinetic mechanism of valeric acid oxidation was proposed. The authors evaluated the rate constants of H-abstraction from the alkyl chain based on the calculations for acetic acid by Cavallotti et al. [60] and taking into account the position and type of each carbon in the chain [61]. Therefore, we also tested our model with the H-abstraction constants from the work of Namysl et al. No significant changes in mole fraction profiles were found, whereas the ROP analysis showed significant differences. According to the model with the constants from Namysl et al., the impact of H-abstraction reaction yielding EPE2J is less than that yielding of EPE3J and EPE4J. Indeed, in [59], the authors discuss the relative impact of H-abstractions in α, β, γ, and δ positions of valeric acid and claim that the oxygenated group inhibits H-abstraction from the α carbon. Such conflicting results indicate the need for additional experimental and theoretical studies of FAEEs with a long alkyl chain.

3.2. Atmospheric-pressure flame

The atmospheric-pressure flat laminar flame of a stoichiometric EPE/O_2/Ar mixture was investigated at the ICKC (Novosibirsk, Russia). The reactants, major intermediates, products, and the main radicals H, OH, and CH_3 were detected using flame- sampling MBMS. The full list of species detected is shown in Table 3.

Formula	Species name	Structure	Formula	Species name	Structure
H	Hydrogen atom	Ḣ	C_2H_4	Ethylene	$H_2C=CH_2$
H_2	Hydrogen	H-H	C_2H_6	Ethane	H_3C-CH_3
OH	Hydroxyl radical	Ȯ-H	CH_2CO	Ketene	$H_2C=C=O$
O_2	Oxygen	O=O	C_3H_6	Propene	$H_2C=CH-CH_3$
CO	Carbon monoxide	C≡O	C_3H_8	Propane	$H_3C-CH_2-CH_3$
CO_2	Carbon dioxide	O=C=O	1,3-C_4H_6	1,3-Butadiene	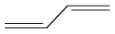
H_2O	Water		CH_2O	Formaldehyde	
CH_3	Methyl radical		CH_3CHO	Acetaldehyde	
CH_4	Methane		C_4H_9COOH	Pentanoic acid	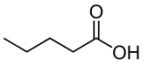
C_2H_2	Acetylene	HC≡CH	$C_7H_{14}O_2$	Ethyl pentanoate	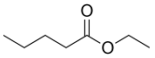

Table 4. List of species detected in the EPE/O_2/Ar flame at atmospheric pressure.

Figure 6 demonstrates a comparison of the measured mole fraction profiles of major stable species and those simulated by the two mechanisms. The experimental temperature profile is also plotted. Both models match the experimental profiles well within the experimental accuracy. Similarly to the low-pressure flame, a small amount of oxygen is presented in the post-flame zone of the atmospheric pressure flame, according to both experiment and simulations. The post-flame temperature is lower in the atmospheric-pressure flame than in the low-pressure flame, due to the higher dilution with inert (see Table 1), the larger sampling probe, and the higher heat transfer to the burner.

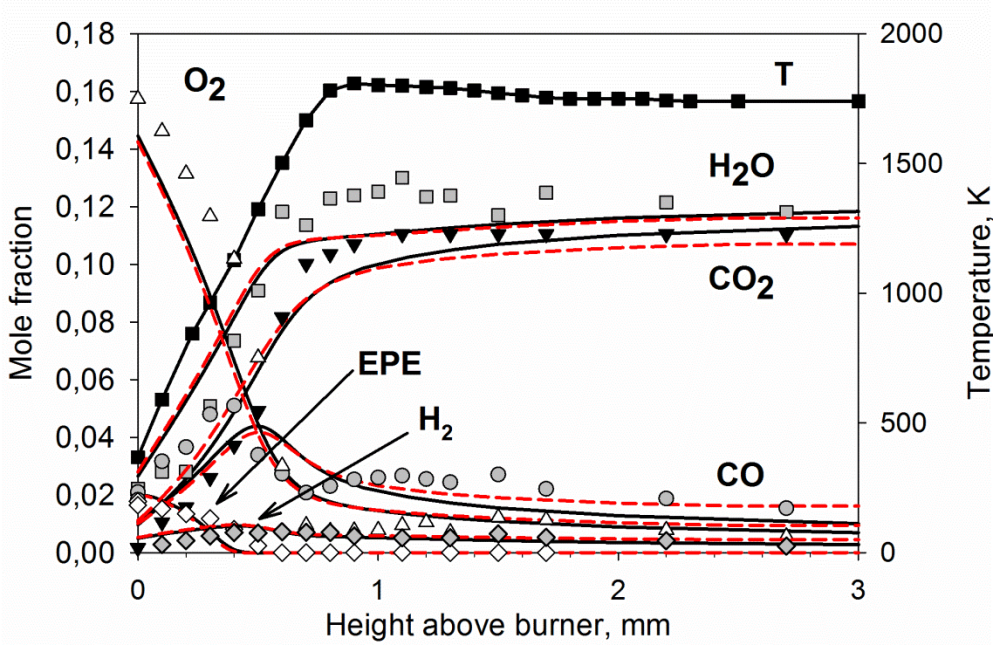

Figure 6. Measured temperature profile and mole fraction profiles of major components in the EPE/O_2/Ar flame at atmospheric pressure. Symbols: experimental data; solid lines: mechanism of Dayma et al.; red dashed lines: present mechanism. The temperature profile is shown by a black solid line with black squares.

Mole fraction profiles of the main flame radicals are shown in Fig. 7. These species are always of great interest due to their decisive role in flames. The experimental mole fraction profiles of OH and CH_3 are in perfect agreement with the calculated ones. The peak mole fraction of atomic hydrogen is several times higher than that predicted by the mechanisms. This is, nevertheless, a satisfactory agreement, since the experimental error of Ḣ quantification is fairly high. Both mechanisms provide very close predictions of the radicals' profiles, but the current model predicts higher H and OH mole fractions in the post-flame zone and a lower peak mole fraction of CH_3. Similar concentrations of radicals in both models confirm that the differences in the impact of H-abstraction reactions are only related to the values of the rate constants involved.

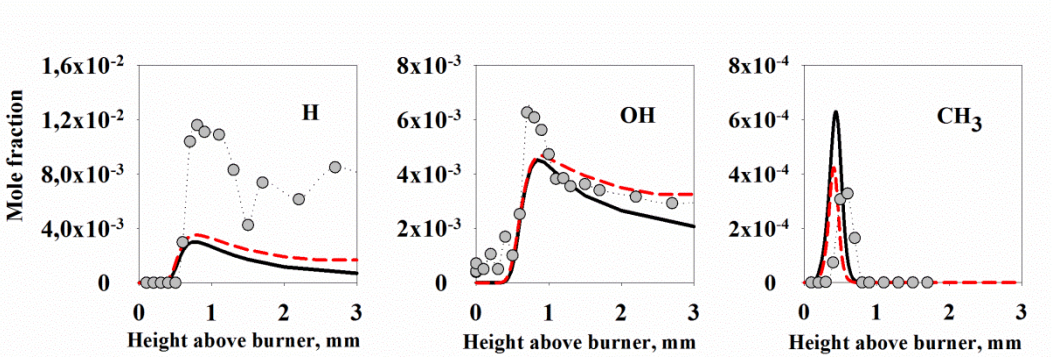

Figure 7. Mole fraction profiles of radicals in the EPE/O_2/Ar flame at 1 atm. Symbols: experimental data; solid lines: mechanism of Dayma et al.; dashed lines: present mechanism.

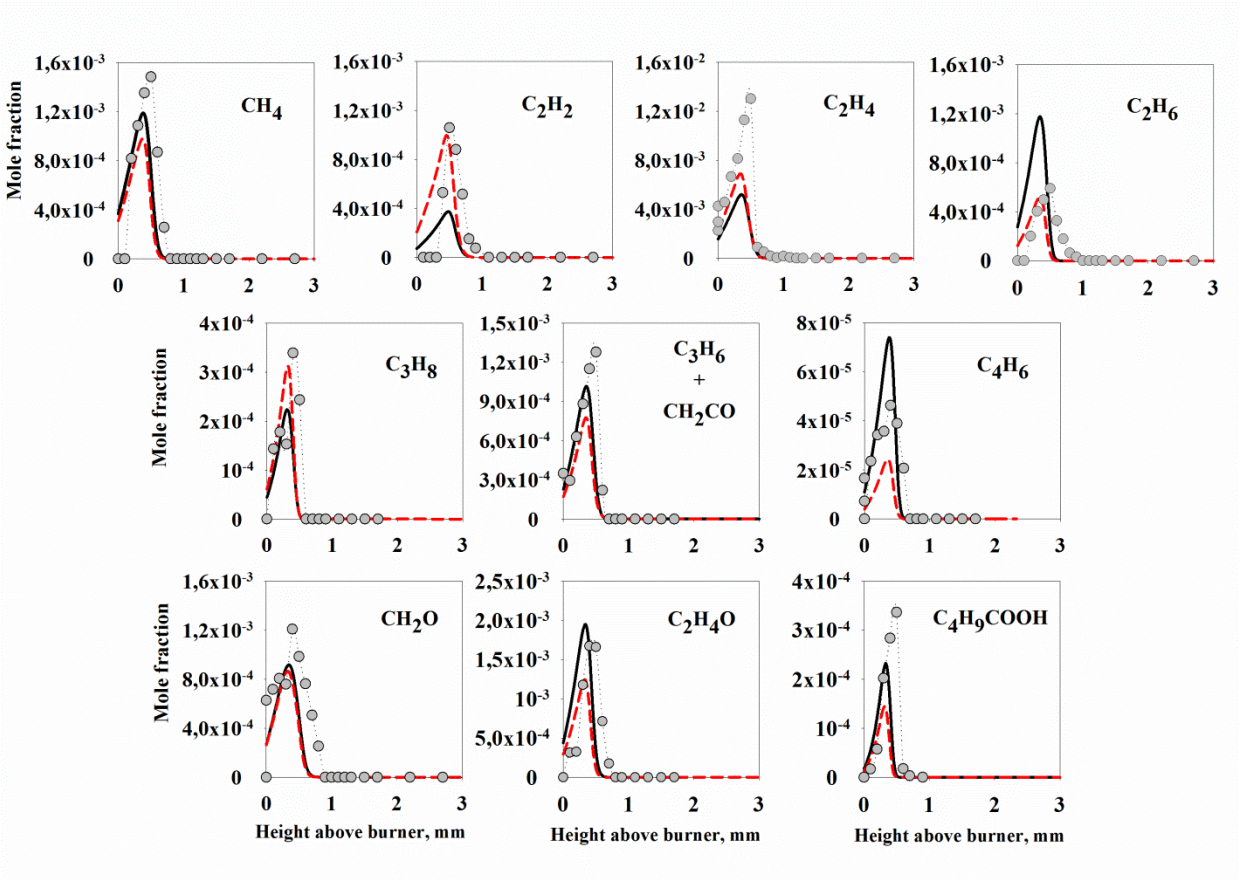

Figure 8. Mole fraction profiles of intermediates in the EPE/O_2/Ar flame at 1 atm. Symbols: experimental data; solid lines: mechanism of Dayma et al.; dashed lines: present mechanism.

Figure 8 shows the experimental and simulated mole fraction profiles of intermediate species detected in the flame at atmospheric pressure. Propene and ketene, which have similar mass-to-charge ratios, were not separated due to very close ionization potentials. Thus, their total mole fraction profile is shown. As can be seen, both models provide a fairly good qualitative reproduction of all experimental data. Predicted mole fraction profiles of methane, propene+ketene, 1,3-butadiene, formaldehyde, and acetaldehyde are also in good quantitative agreement with measurements within the experimental error.

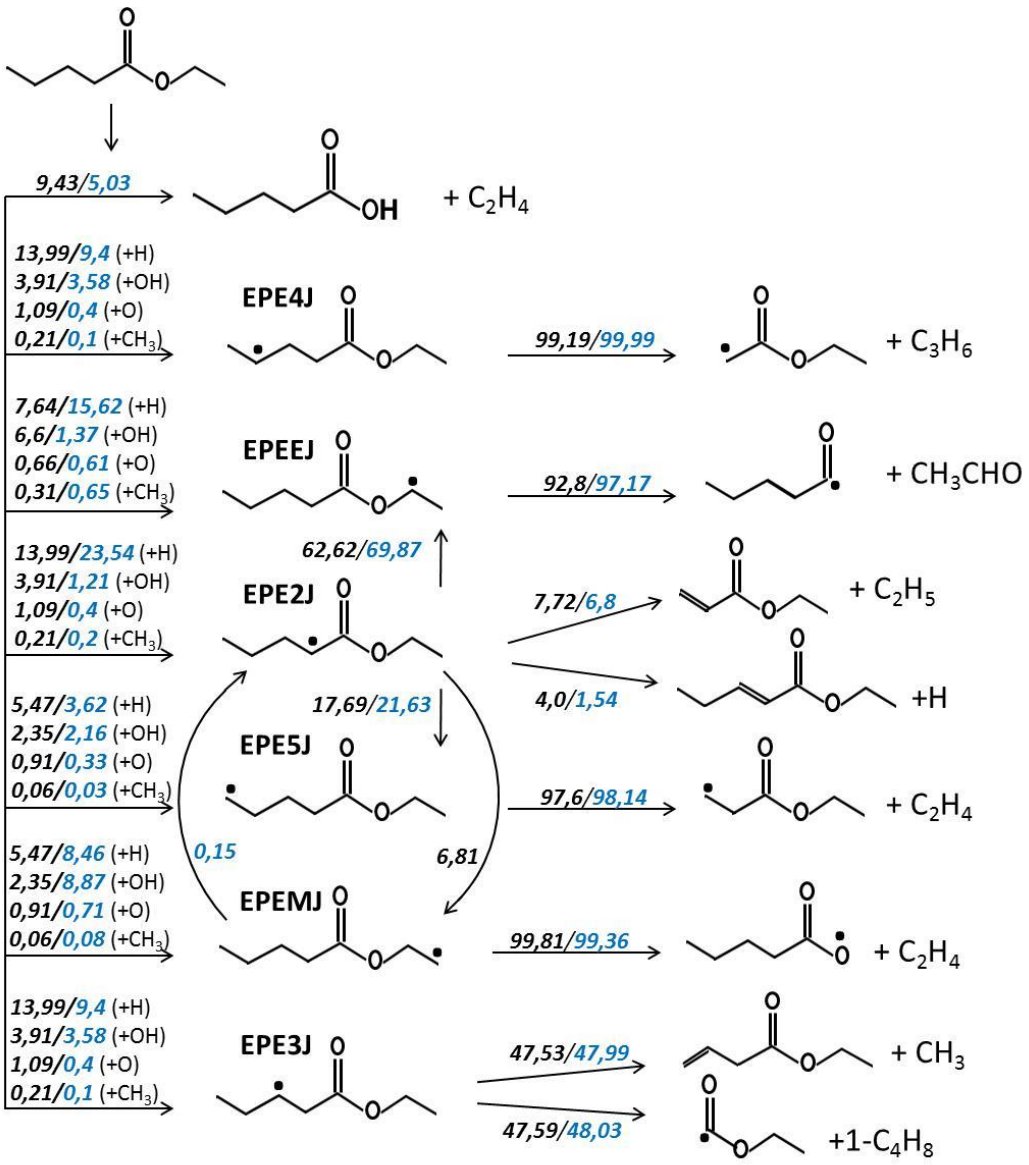

Figure 9. Integrated ROP analysis of the primary pathways of EPE destruction at atmospheric pressure. Black values: percentage contribution to the total consumption of a particular component according to the model of Dayma et al.; blue values: according to the present model.

The mole fraction profiles of acetaldehyde, ethane and propane predicted by the present mechanism are in very good quantitative agreement with the experimental ones. As in the low-pressure flame, in the flame at 1 atm, the current mechanism predicts the C_2H_2 peak mole fraction better than the Dayma et al. mechanism. As in the low-pressure flame, the peak mole fraction of 1,3-butadiene is slightly underestimated by the present model and overestimated by the mechanism of Dayma et al.

The measured peak mole fraction of ethylene in the atmospheric pressure flame, as in the low-pressure flame, is nearly twice higher than the models' predictions. This gives an indication

of inaccuracies in ethylene kinetics in both models. Ethylene is formed in many primary pathways of EPE destruction; therefore, a further revision of the kinetics of formation and consumption of the fuel radicals is needed first of all. MBMS is a more reliable method than microprobe sampling in terms of conservation of the composition of the sampled gases. For this reason in the flame at 1 atm, unlike in the low-pressure flame, the uncertainty in the measurement of the valeric acid profile is considerably lower. The peak mole fraction of the acid is predicted by the mechanism of Dayma et al. within experimental errors. Our mechanism underestimates its peak mole fraction by a factor of almost 3. This may be due to a decrease of the role of unimolecular decomposition in our mechanism under atmospheric pressure conditions. As seen from the integrated ROP analysis for the flame at 1 atm (Fig. 9), the contribution of the unimolecular decomposition of EPE in the mechanism of Dayma et al. is almost two times higher than that in our mechanism. This leads to a lower concentration of the acid compared to the concentration of primary fuel radicals. The distribution of the percentage contributions of H-atom abstraction pathways is similar to that in the low-pressure flame. The H-atom abstraction reactions in positions *2, 3*, and *4* are the most important in the mechanism of Dayma, as in the case of the low-pressure flame. According to our mechanism, the contribution of H-atom abstraction pathways in positions *2* and *E* is most significant, which is directly related to the use of the revised rate constants for these reactions.

With an increase in pressure, marked differences between these two mechanisms are observed in the contribution of isomerization reactions:

(1) EPE2J ⇆ EPEEJ
(2) EPE2J ⇆ EPE5J
(3) EPE2J ⇆ EPEMJ

The contribution of reaction (1) increased from 44% at low pressure to 63% at 1 atm in the mechanism of Dayma et al., but in our mechanism, it increased only by 5%. The impact of reaction (2) decreased by 7.5% and 2.7% in the mechanism of Dayma et al. and the present mechanism, respectively. The impact of reaction (3) is negligible in our mechanism for both pressures, whereas in the mechanism of Dayma et al., its impact was 14% at low pressure and almost 7% at atmospheric pressure. These isomerizations play a significant role in the redistribution of fuel consumption pathways and therefore affect the resulting pool of short intermediates.

Both mechanisms demonstrated advantages and disadvantages in predictions of different intermediates. One can conclude that in the case of atmospheric pressure conditions, the present mechanism performs better. Some shortcomings of our mechanism indicate the need for further theoretical calculations of the kinetic parameters of H-atom abstractions and unimolecular decompositions of EPE and EB. Such calculations could also help to understand pressure effects, which are essential for practical use. In particular, it should be noted that with a pressure rise, the ratio of the H and OH concentrations in the flames is expected to decrease due to the increasing contribution of the reaction $H+O_2(+M)⇆HO_2(+M)$ producing HO_2, which decomposes mainly in the reaction $HO_2+H⇆OH+OH$ [62,63]. Therefore, the H-abstraction reactions from fuel (and other intermediates) by OH attack are expected to play a more significant role at a pressure above 1 atm. Therefore, additional experimental studies of thecombustion of valeric fuels at elevated pressures are also required to validate the assumptions and to further improve the predictive capability of the mechanism.

3.3. Laminar burning velocity of EPE/air mixtures

The mechanism of Dayma et al. was validated against experimental data on the burning velocity of EPE/air mixtures at different equivalence ratios and pressures [26]. Since the laminar flame speed is one of the most important combustion parameters, in this work we also validated our mechanism against the flame speed data of Dayma et al. Figure 10 demonstrates a comparison of experimental and modeling data from [26] and model predictions using the present mechanism. The initial temperature of the mixtures T_i was 423 K at pressures of 1, 3, and 5 bar. The equivalence ratios were varied from 0.7 to 1.4 at 1 and 3 bar, and from 0.8 to 1.0 at 5 bar. The experimental error was ±2 cm/s [26]. As is seen, the laminar burning velocity at 1 bar is predicted by both mechanisms very similarly in the whole range of equivalence ratios.

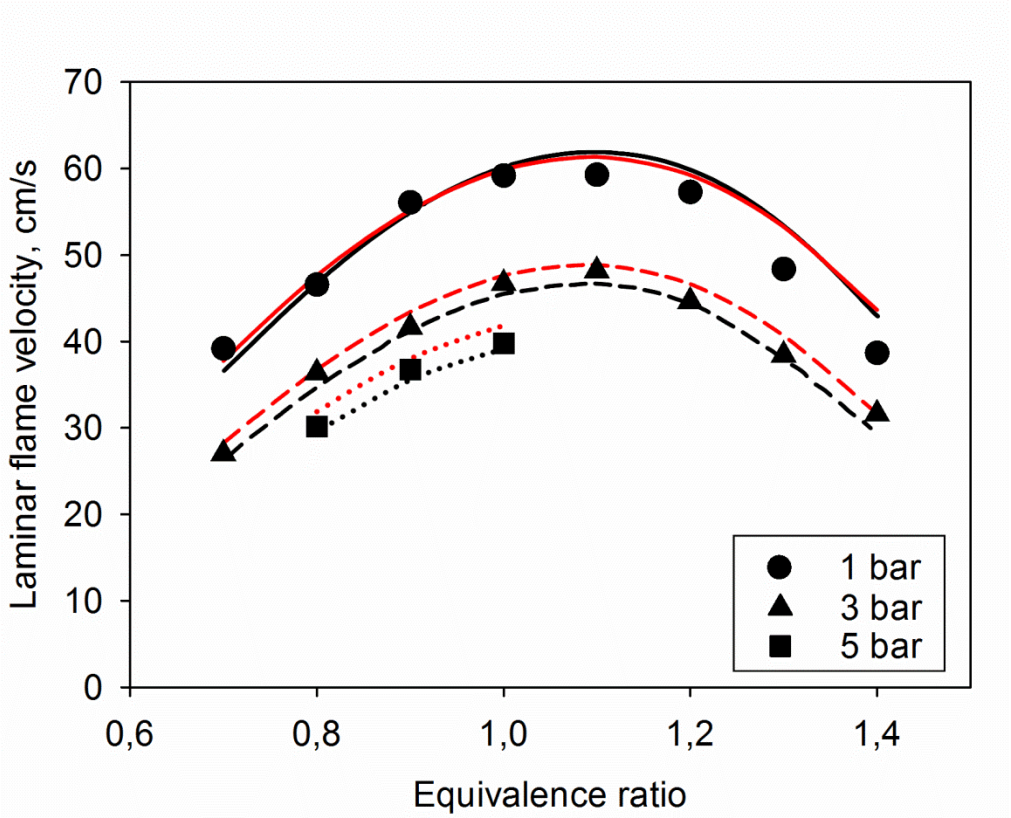

Figure 10. Laminar burning velocities of EPE/air mixtures at different equivalence ratios and pressures, initial mixture temperature T_i=423 K. Symbols: experimental data; black lines: mechanism of Dayma et al.; red lines: present mechanism.

The simulated burning velocity is in perfect agreement with the experiment for lean and stoichiometric mixtures, but both mechanisms slightly overestimate the burning velocity of fuel-rich blends. At 3 and 5 bars, the present mechanism predicts slightly higher values of burning velocity than those given by the Dayma et al. mechanism. However, the predictions by both mechanisms diverge only by 2 cm/s, which is within the experimental error.

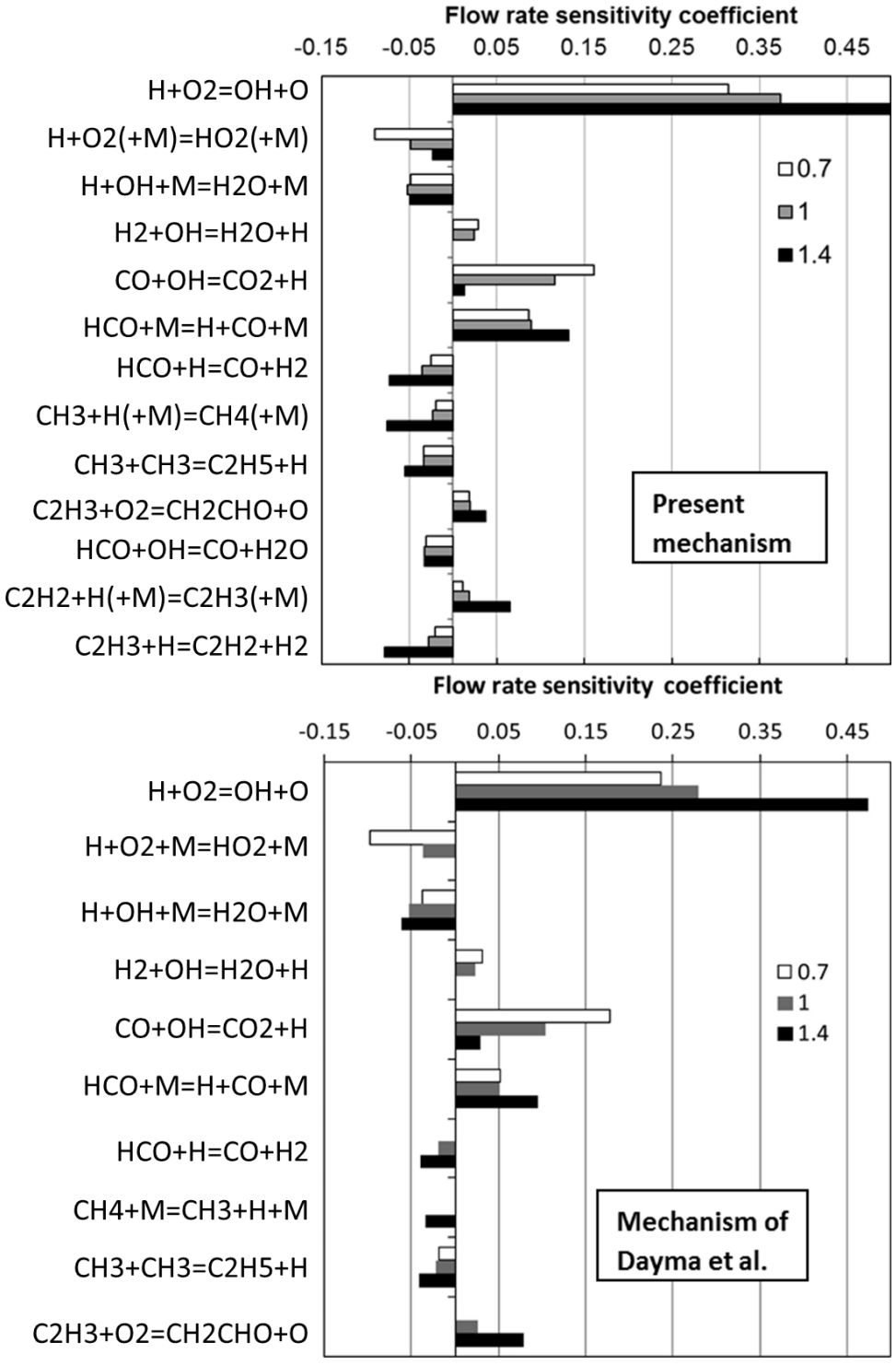

Figure 11. Flow rate sensitivity analysis of both mechanisms for EPE/air mixtures under lean (φ=0.7), stoichiometric (φ =1), and fuel-rich (φ =1.4) conditions.

To compare both mechanisms, we performed a sensitivity analysis for the present mechanism. (Fig. 11). Flow rate sensitivity coefficients were calculated in the same manner as in

the work of Dayma et al.: at atmospheric pressure, T_i=423 K, and equivalence ratios 0.7, 1.0, and 1.4. As expected, the burning velocity is most sensitive, according to both mechanisms, to the rate constants of the reactions $H+O_2=OH+O$ and $CO+OH=CO_2+H$. In addition to these reactions, the most important reactions in both mechanisms are $H+O_2+M=HO_2+M$, $H+OH+M=H_2O+M$ and $HCO+H=CO+H_2$. Thus, as in the case of shorter esters [12], the laminar flame speed of EPE is controlled by the basic H_2/O_2 and C_0-C_2 kinetics. Despite the significant effort focused on its study, there is still no consensus on this issue and hence on the conventional set of corresponding reaction rate constants [64]. In the mechanism of Dayma et al. and the Aramco 1.3 mechanism, these basic sets are slightly different, particularly in terms of pressure dependence. The sensitivity analysis shows that the kinetics of acetylene and vinyl radical play a more prominent role in our mechanism, especially under fuel-rich conditions. This is reasonable because EPE produces a lot of ethylene (see Fig. 5 and 9). It seems that the kinetics of the $C_2H_4 \rightarrow C_2H_3 \rightarrow C_2H_2$ transformations is better described in our mechanism, due to the use of AramcoMech 1.3.

4. Conclusion

An updated chemical kinetic mechanism for EPE combustion was proposed in this work. The mechanism includes the most recent rate constants of the most important reactions, including their pressure dependencies, and it is certainly able to reproduce the main trends in the combustion kinetics of lighter ethyl esters with an alkyl chain from C_0 to C_5.

The mechanism was validated against the new experimental data reported in this paper on the chemical speciation of two laminar premixed stoichiometric EPE/O_2/Ar flames stabilized on flat flame burners at low (50 Torr) and atmospheric pressures. The proposed mechanism was shown to reproduce well this set of experimental data, especially at atmospheric pressure. The new mechanism was also shown to reproduce well literature experimental data for laminar burning velocities of EPE/air mixtures at pressures of 1-5 bar. Therefore, the mechanism proposed can be used for the development of predictive kinetic models for the combustion of ethyl-ester based biofuels.

The observed discrepancies between predictions and observations for some flame intermediates indicate the need for refinement of the rate constants of H-atom abstraction reactions by H and OH radicals in the *M*, *E* and 2^{nd} positions of the EPE molecule. Further revision of decomposition pathways of fuel radicals is also needed. Although the experimental data reported in this paper extend the available experimental database for the combustion of ethyl esters, further experimental investigations of the combustion of EPE and other ethyl esters, especially at elevated pressures, are needed to develop a reliable kinetic model for the combustion of transportation fuels based on ethyl esters.

5. Acknowledgements

This work was supported financially by the Ministry of Science and Higher Education of the Russian Federation (project №075-15-2019-1878).

6. References

[1] Atabani AE, Silitonga AS, Badruddin IA, Mahlia TMI, Masjuki HH, Mekhilef S. A comprehensive review on biodiesel as an alternative energy resource and its characteristics. Renew Sustain Energy Rev 2012;16:2070–93. https://doi.org/10.1016/j.rser.2012.01.003.

[2] Coniglio L, Bennadji H, Glaude PA, Herbinet O, Billaud F. Combustion chemical kinetics of biodiesel and related compounds (methyl and ethyl esters): Experiments and modeling – Advances and future refinements. Prog Energy Combust Sci 2013;39:340–82. https://doi.org/10.1016/j.pecs.2013.03.002.

[3] Sadeghinezhad E, Kazi SN, Sadeghinejad F, Badarudin A, Mehrali M, Sadri R, et al. A comprehensive literature review of bio-fuel performance in internal combustion engine and relevant costs involvement. Renew Sustain Energy Rev 2014;30:29–44. https://doi.org/10.1016/j.rser.2013.09.022.

[4] Brunschwig C, Moussavou W, Blin J. Use of bioethanol for biodiesel production. Prog Energy Combust Sci 2012;38:283–301. https://doi.org/10.1016/j.pecs.2011.11.001.

[5] Nitièma-Yefanova S, Coniglio L, Schneider R, Nébié RHC, Bonzi-Coulibaly YL. Ethyl biodiesel production from non-edible oils of Balanites aegyptiaca, Azadirachta indica, and Jatropha curcas seeds – Laboratory scale development. Renew Energy 2016;96:881–90. https://doi.org/10.1016/j.renene.2016.04.100.

[6] Metcalfe WK, Dooley S, Curran HJ, Simmie JM, El-Nahas AM, Navarro MV. Experimental and Modeling Study of C5H10O2 Ethyl and Methyl Esters. J Phys Chem A 2007;111:4001–14. https://doi.org/10.1021/jp067582c.

[7] Hakka MH, Bennadji H, Biet J, Yahyaoui M, Sirjean B, Warth V, et al. Oxidation of methyl and ethyl butanoates. Int J Chem Kinet 2010;42:226–52. https://doi.org/10.1002/kin.20473.

[8] Akih-Kumgeh B. Experimental and Modeling Study of Trends in the High-Temperature Ignition of Methyl and Ethyl Esters. Energy Fuels 2011;25:4345–56. https://doi.org/10.1021/ef200977p.

[9] Ren W, Mitchell Spearrin R, Davidson DF, Hanson RK. Experimental and Modeling Study of the Thermal Decomposition of C3–C5 Ethyl Esters Behind Reflected Shock Waves. J Phys Chem A 2014;118:1785–98. https://doi.org/10.1021/jp411766b.

[10] Metcalfe WK, Togbé C, Dagaut P, Curran HJ, Simmie JM. A jet-stirred reactor and kinetic modeling study of ethyl propanoate oxidation. Combust Flame 2009;156:250–60. https://doi.org/10.1016/j.combustflame.2008.09.007.

[11] Belloche A, Garrod RT, Müller HSP, Menten KM, Comito C, Schilke P. Increased complexity in interstellar chemistry: detection and chemical modeling of ethyl formate and n-propyl cyanide in Sagittarius B2(N). Astron Astrophys 2009;499:215–32. https://doi.org/10.1051/0004-6361/200811550.

[12] Wang YL, Lee DJ, Westbrook CK, Egolfopoulos FN, Tsotsis TT. Oxidation of small alkyl esters in flames. Combust Flame 2014;161:810–7. https://doi.org/10.1016/j.combustflame.2013.09.013.

[13] Osswald P, Struckmeier U, Kasper T, Kohse-Höinghaus K, Wang J, Cool TA, et al. Isomer-Specific Fuel Destruction Pathways in Rich Flames of Methyl Acetate and Ethyl Formate and Consequences for the Combustion Chemistry of Esters. J Phys Chem A 2007;111:4093–101. https://doi.org/10.1021/jp068337w.

[14] Sun W, Tao T, Zhang R, Liao H, Huang C, Zhang F, et al. Experimental and modeling efforts towards a better understanding of the high-temperature combustion kinetics of C3C5 ethyl esters. Combust Flame 2017;185:173–87. https://doi.org/10.1016/j.combustflame.2017.07.013.
[15] Westbrook CK, Pitz WJ, Westmoreland PR, Dryer FL, Chaos M, Osswald P, et al. A detailed chemical kinetic reaction mechanism for oxidation of four small alkyl esters in laminar premixed flames. Proc Combust Inst 2009;32:221–8. https://doi.org/10.1016/j.proci.2008.06.106.
[16] Ning H, Wu J, Ma L, Ren W, Davidson DF, Hanson RK. Combined Ab Initio, Kinetic Modeling, and Shock Tube Study of the Thermal Decomposition of Ethyl Formate. J Phys Chem A 2017;121:6568–79. https://doi.org/10.1021/acs.jpca.7b05382.
[17] Badawy T, Williamson J, Xu H. Laminar burning characteristics of ethyl propionate, ethyl butyrate, ethyl acetate, gasoline and ethanol fuels. Fuel 2016;183:627–40. https://doi.org/10.1016/j.fuel.2016.06.087.
[18] Dayma G, Halter F, Foucher F, Mounaim-Rousselle C, Dagaut P. Laminar Burning Velocities of C4–C7 Ethyl Esters in a Spherical Combustion Chamber: Experimental and Detailed Kinetic Modeling. Energy Fuels 2012;26:6669–77. https://doi.org/10.1021/ef301254q.
[19] Gasnot L, Decottignies V, Pauwels JF. Ethyl acetate oxidation in flame condition: an experimental study. Fuel 2004;83:463–70. https://doi.org/10.1016/j.fuel.2003.10.008.
[20] Yang B, Westbrook CK, Cool TA, Hansen N, Kohse-Höinghaus K. Fuel-specific influences on the composition of reaction intermediates in premixed flames of three C5H10O2 ester isomers. Phys Chem Chem Phys 2011;13:6901–13. https://doi.org/10.1039/C0CP02065F.
[21] Osipova KN, Dmitriev AM, Shmakov AG, Korobeinichev OP, Minaev SS, Knyazkov DA. Combustion of ethyl acetate: the experimental study of flame structure and validation of chemical kinetic mechanisms. Mendeleev Commun 2019;29:690–2. https://doi.org/10.1016/j.mencom.2019.11.030.
[22] Schwartz WR, McEnally CS, Pfefferle LD. Decomposition and Hydrocarbon Growth Processes for Esters in Non-Premixed Flames. J Phys Chem A 2006;110:6643–8. https://doi.org/10.1021/jp0549576.
[23] Ahmed A, Pitz WJ, Cavallotti C, Mehl M, Lokachari N, Nilsson EJK, et al. Small ester combustion chemistry: Computational kinetics and experimental study of methyl acetate and ethyl acetate. Proc Combust Inst 2018. https://doi.org/10.1016/j.proci.2018.06.178.
[24] Bennadji H, Glaude PA, Coniglio L, Billaud F. Experimental and kinetic modeling study of ethyl butanoate oxidation in a laminar tubular plug flow reactor. Fuel 2011;90:3237–53. https://doi.org/10.1016/j.fuel.2011.06.028.
[25] Dmitriev AM, Osipova KN, Knyazkov DA, Gerasimov IE, Shmakov AG, Korobeinichev OP. Comparative Analysis of the Chemical Structure of Ethyl Butanoate and Methyl Pentanoate Flames. Combust Explos Shock Waves 2018;54:125–35. https://doi.org/10.1134/S0010508218020016.
[26] Dayma G, Halter F, Foucher F, Togbé C, Mounaim-Rousselle C, Dagaut P. Experimental and Detailed Kinetic Modeling Study of Ethyl Pentanoate (Ethyl Valerate) Oxidation in a Jet Stirred Reactor and Laminar Burning Velocities in a Spherical Combustion Chamber. Energy Fuels 2012;26:4735–48. https://doi.org/10.1021/ef300581q.
[27] Contino F, Foucher F, Halter F, Dayma G, Dagaut P, Mounaïm-Rousselle C. Engine Performances and Emissions of Second-Generation Biofuels in Spark Ignition Engines: The

Case of Methyl and Ethyl Valerates. SAE Tech Pap 2013;2013-24–0098. https://doi.org/10.4271/2013-24-0098.
[28] Knyazkov DA, Gerasimov IE, Hansen N, Shmakov AG, Korobeinichev OP. Photoionization mass spectrometry and modeling study of a low-pressure premixed flame of ethyl pentanoate (ethyl valerate). Proc Combust Inst 2017;36:1185–92. https://doi.org/10.1016/j.proci.2016.07.038.
[29] Katshiatshia HM, Dias V, Jeanmart H. Experimental and Numerical Study of Ethyl Valerate Flat Flames at Low Pressure. Combust Sci Technol 2018;190:632–62. https://doi.org/10.1080/00102202.2017.1403910.
[30] Zhang Y, Boehman AL. Experimental study of the autoignition of C8H16O2 ethyl and methyl esters in a motored engine. Combust Flame 2010;157:546–55. https://doi.org/10.1016/j.combustflame.2009.09.003.
[31] Diévart P, Gong J, Ju Y. A Comparative Study of the Kinetics of Ethyl and Methyl Esters in Diffusion Flame Extinction. Proc ASME 2013 Heat Transf Summer Conf 2013:V002T05A005. https://doi.org/10.1115/ht2013-17086.
[32] Ghosh MK, Howard MS, Zhang Y, Djebbi K, Capriolo G, Farooq A, et al. The combustion kinetics of the lignocellulosic biofuel, ethyl levulinate. Combust Flame 2018;193:157–69. https://doi.org/10.1016/j.combustflame.2018.02.028.
[33] Boot M. Biofuels from Lignocellulosic Biomass. Biofuels Lignocellul. Biomass, John Wiley & Sons, Ltd; 2016, p. 209–14. https://doi.org/10.1002/9783527685318.index.
[34] Lange J-P, Price R, Ayoub PM, Louis J, Petrus L, Clarke L, et al. Valeric Biofuels: A Platform of Cellulosic Transportation Fuels. Angew Chem Int Ed 2010;49:4479–83. https://doi.org/10.1002/anie.201000655.
[35] Zhou J, Zhu R, Deng J, Fu Y. Preparation of valeric acid and valerate esters from biomass-derived levulinic acid using metal triflates + Pd/C. Green Chem 2018;20:3974–80. https://doi.org/10.1039/c8gc01606b.
[36] Dias V, Katshiatshia HM, Jeanmart H. The influence of ethanol addition on a rich premixed benzene flame at low pressure. Combust Flame 2014;161:2297–304. https://doi.org/10.1016/j.combustflame.2014.03.005.
[37] Pousse E, Glaude PA, Fournet R, Battin-Leclerc F. A lean methane premixed laminar flame doped with components of diesel fuel: I. n-Butylbenzene. Combust Flame 2009;156:954–74. https://doi.org/10.1016/j.combustflame.2008.09.012.
[38] Tran L-S, Verdicchio M, Monge F, Martin RC, Bounaceeur R, Sirjean B, et al. An experimental and modeling study of the combustion of tetrahydrofuran. Combust Flame 2015;162:1899–918. https://doi.org/10.1016/j.combustflame.2014.12.010.
[39] Kint JH. A noncatalytic coating for platinum-rhodium thermocouples. Combust Flame 1970;14:279–81. https://doi.org/10.1016/S0010-2180(70)80040-2.
[40] Bonne U, Grewer Th, Wagner HG. Messungen in der Reaktionszone von Wasserstoff—Sauerstoff- und Methan—Sauerstoff-Flammen. Z Für Phys Chem 1960;26:93–110. https://doi.org/10.1524/zpch.1960.26.1_2.093.
[41] Gerasimov IE, Knyazkov DA, Yakimov SA, Bolshova TA, Shmakov AG, Korobeinichev OP. Structure of atmospheric-pressure fuel-rich premixed ethylene flame with and without ethanol. Combust Flame 2012;159:1840–50. https://doi.org/10.1016/j.combustflame.2011.12.022.
[42] Dmitriev AM, Knyazkov DA, Bolshova TA, Shmakov AG, Korobeinichev OP. The effect of methyl pentanoate addition on the structure of premixed fuel-rich n-heptane/toluene

flame at atmospheric pressure. Combust Flame 2015;162:1964–75. https://doi.org/10.1016/j.combustflame.2014.12.015.
[43] Botha J. P., Spalding Dudley Brian, Egerton Alfred Charles. The laminar flame speed of propane/air mixtures with heat extraction from the flame. Proc R Soc Lond Ser Math Phys Sci 1954;225:71–96. https://doi.org/10.1098/rspa.1954.0188.
[44] Cool TA, Nakajima K, Taatjes CA, McIlroy A, Westmoreland PR, Law ME, et al. Studies of a fuel-rich propane flame with photoionization mass spectrometry. Proc Combust Inst 2005;30:1681–8. https://doi.org/10.1016/j.proci.2004.08.103.
[45] Y.-K. Kim, K.K. Irikura, M.E. Rudd, M.A. Ali, P.M. Stone. Electron-Impact Cross Sections for Ionization and Excitation Database. NIST 2009. https://www.nist.gov/pml/electron-impact-cross-sections-ionization-and-excitation-database (accessed October 26, 2016).
[46] Kaskan WE. The dependence of flame temperature on mass burning velocity. Proc Combust Inst 1957;6:134–43. https://doi.org/10.1016/S0082-0784(57)80021-6.
[47] Shaddix CR. Correcting Thermocouple Measurements for Radiation Loss: A Critical Review. Sandia National Labs., Livermore, CA (US); 1999.
[48] Kee RJ, Rupley FM, Miller JA. Chemkin-II: A Fortran Chemical Kinetics Package for the Analysis of Gas-Phase Chemical Kinetics. Sandia National Labs., Livermore, CA (USA); 1989.
[49] Dagaut P, Togbé C. Experimental and Modeling Study of the Kinetics of Oxidation of Ethanol−Gasoline Surrogate Mixtures (E85 Surrogate) in a Jet-Stirred Reactor. Energy Fuels 2008;22:3499–505. https://doi.org/10.1021/ef800214a.
[50] Sarathy SM, Thomson MJ, Togbé C, Dagaut P, Halter F, Mounaim-Rousselle C. An experimental and kinetic modeling study of n-butanol combustion. Combust Flame 2009;156:852–64. https://doi.org/10.1016/j.combustflame.2008.11.019.
[51] Dayma G, Togbé C, Dagaut P. Experimental and Detailed Kinetic Modeling Study of Isoamyl Alcohol (Isopentanol) Oxidation in a Jet-Stirred Reactor at Elevated Pressure. Energy Fuels 2011;25:4986–98. https://doi.org/10.1021/ef2012112.
[52] Metcalfe WK, Burke SM, Ahmed SS, Curran HJ. A Hierarchical and Comparative Kinetic Modeling Study of C1 − C2 Hydrocarbon and Oxygenated Fuels. Int J Chem Kinet 2013;45:638–75. https://doi.org/10.1002/kin.20802.
[53] Marinov NM. A detailed chemical kinetic model for high temperature ethanol oxidation. Int J Chem Kinet 1999;31:183–220. https://doi.org/10.1002/(SICI)1097-4601(1999)31:3<183::AID-KIN3>3.0.CO;2-X.
[54] Wang Q-D, Wang X-J, Liu Z-W, Kang G-J. Theoretical and kinetic study of the hydrogen atom abstraction reactions of ethyl esters with hydrogen radicals. Chem Phys Lett 2014;616–617:109–14. https://doi.org/10.1016/j.cplett.2014.10.032.
[55] Mendes J, Zhou C-W, Curran HJ. Theoretical Study of the Rate Constants for the Hydrogen Atom Abstraction Reactions of Esters with •OH Radicals. J Phys Chem A 2014;118:4889–99. https://doi.org/10.1021/jp5029596.
[56] Tan T, Yang X, Ju Y, Carter EA. Ab initio kinetics studies of hydrogen atom abstraction from methyl propanoate. Phys Chem Chem Phys 2016;18:4594–607. https://doi.org/10.1039/C5CP07282D.
[57] Korobeinichev OP, Gerasimov IE, Knyazkov DA, Shmakov AG, Bolshova TA, Hansen N, et al. An Experimental and Kinetic Modeling Study of Premixed Laminar Flames of Methyl

Pentanoate and Methyl Hexanoate. Z Für Phys Chem 2015;229:759–80. https://doi.org/10.1515/zpch-2014-0596.
[58] Gerasimov IE, Knyazkov DA, Dmitriev AM, Kuibida LV, Shmakov AG, Korobeinichev OP. Experimental and numerical study of the structure of a premixed methyl decanoate/oxygen/argon flame. Combust Explos Shock Waves 2015;51:285–92. https://doi.org/10.1134/S0010508215030016.
[59] Namysl S, Pelucchi M, Herbinet O, Frassoldati A, Faravelli T, Battin-Leclerc F. A first evaluation of butanoic and pentanoic acid oxidation kinetics. Chem Eng J 2019;373:973–84. https://doi.org/10.1016/j.cej.2019.05.090.
[60] Cavallotti C, Pelucchi M, Frassoldati A. Analysis of acetic acid gas phase reactivity: Rate constant estimation and kinetic simulations. Proc Combust Inst 2019;37:539–46. https://doi.org/10.1016/j.proci.2018.06.137.
[61] RANZI El, DENTE M, FARAVELLI T, PENNATI G. Prediction of Kinetic Parameters for Hydrogen Abstraction Reactions. Combust Sci Technol 1993;95:1–50. https://doi.org/10.1080/00102209408935325.
[62] Dmitriev AM, Knyazkov DA, Bolshova TA, Tereshchenko AG, Paletsky AA, Shmakov AG, et al. Structure of CH4/O2/Ar flames at elevated pressures studied by flame sampling molecular beam mass spectrometry and numerical simulation. Combust Flame 2015;162:3946–59. https://doi.org/10.1016/j.combustflame.2015.07.032.
[63] Knyazkov DA, Dmitriev AM, Bolshova TA, Shvartsberg VM, Shmakov AG, Korobeinichev OP. Structure of premixed H2/O2/Ar flames at 1–5 atm studied by molecular beam mass spectrometry and numerical simulation. Proc Combust Inst 2017;36:1233–40. https://doi.org/10.1016/j.proci.2016.07.109.
[64] Curran HJ. Developing detailed chemical kinetic mechanisms for fuel combustion. Proc Combust Inst 2019;37:57–81. https://doi.org/10.1016/j.proci.2018.06.054.